

# GFD 2012 Lecture 4 Part I: Structures in 3D quasi-geostrophic flows

Jeffrey B. Weiss; notes by Alban Sauret and Vamsi Krishna Chalamalla

June 21, 2012

## 1 Introduction

Geostrophic fluid dynamics describes a flow in which the force due to pressure gradient balances the Coriolis force. The large-scale flows in the atmosphere and ocean are approximately in geostrophic balance. Many studies show that the QG decaying turbulence self-organizes into roughly spherical vortices. Dynamical evolution of these vortices such as merging and alignment processes are interesting. Results of numerical investigations which studied the evolution processes such as merging and alignment are discussed in the following sections [1, 2].

## 2 Vortex merging

Similar to the two-dimensional decaying turbulence, quasi-geostrophic three-dimensional turbulence leads to same sign vortex merging, which is an important mechanism in determining the flow evolution.

### 2.1 Numerical method and initial condition

Numerical simulations are performed to study the dynamics of vortex merging process and also the effects of varying the aspect ratio on the merging process [1]. The following equation for potential vorticity has been solved numerically.

$$\frac{\partial q}{\partial t} + J(\psi, q) = \mathfrak{D}, \quad (1)$$

where

$$J(\psi, q) = \frac{\partial \psi}{\partial x} \frac{\partial q}{\partial y} - \frac{\partial \psi}{\partial y} \frac{\partial q}{\partial x}, \quad (2)$$

is the Jacobian operator,  $\psi$  is the stream function and the potential vorticity  $q$  is defined as

$$q = \frac{\partial^2 \psi}{\partial x^2} + \frac{\partial^2 \psi}{\partial y^2} + \frac{\partial^2 \psi}{\partial z'^2}, \quad (3)$$

where  $z'$  is the rescaled vertical coordinate,  $z' = (N/f)z$ .  $\mathfrak{D}$  on the right hand side of the potential vorticity equation represents the dissipation term, which is assumed to be

small compared to the other terms. Simulations are performed in a domain of size  $2\pi$  in the horizontal directions and  $D$  in the vertical direction, where  $D=2\pi$  in all simulations except those with the smallest aspect ratio  $H/R=0.16$  where  $D=\pi/2$ . Periodic boundary conditions are used in all the three directions. The initial condition for potential vorticity is given by two ellipsoidal distributions with circular horizontal cross-sections of radius  $R$  and half-height  $H$ . Figure 1 shows the initial potential vorticity distribution. The vorticity field is symmetric with respect to the mid-plane  $z'_c = D/2$ .

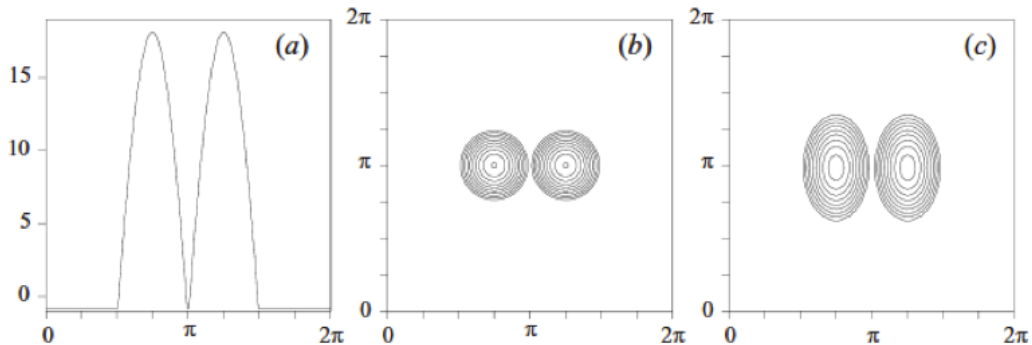


Figure 1: Initial potential vorticity distribution (a) the cosine profile of the vortices (b) horizontal PV section on the mid-plane (c) vertical PV section on the plane  $(x,z)$ .

## 2.2 Results

Figure 2 shows the time evolution of the vorticity field for one of the simulated case with aspect ratio  $H/R = 1.5$ . Figure 2(a) shows the potential vorticity field at a horizontal section  $z'_c = D/2$ . Figure 2(b) shows PV distribution at  $z'_1 = z'_c + 3H/4$ , whereas figure 2(c) shows the PV distribution at a vertical section  $y = \pi$ . The horizontal section of PV distribution at  $z'_c = D/2$  shows the vortices merging to form a core with thin filaments around the core. Vertical section of PV distribution shows that these filaments are actually an ensemble of 'PV sheets' which enclose the merging vortices. Horizontal section of PV distribution at  $z'_1$  shows that there is no definite core at this vertical level and the vorticity has been elongated to form spiral like shape. Overall, the evolution leads to an increase in the final radius and decrease in the vortex height thus reducing the aspect ratio. Another interesting dynamics of the vortex cores is that they elongate to form a flattened core before merging. Figure 3 shows the three-dimensional volume rendering of the PV field at different time instances.

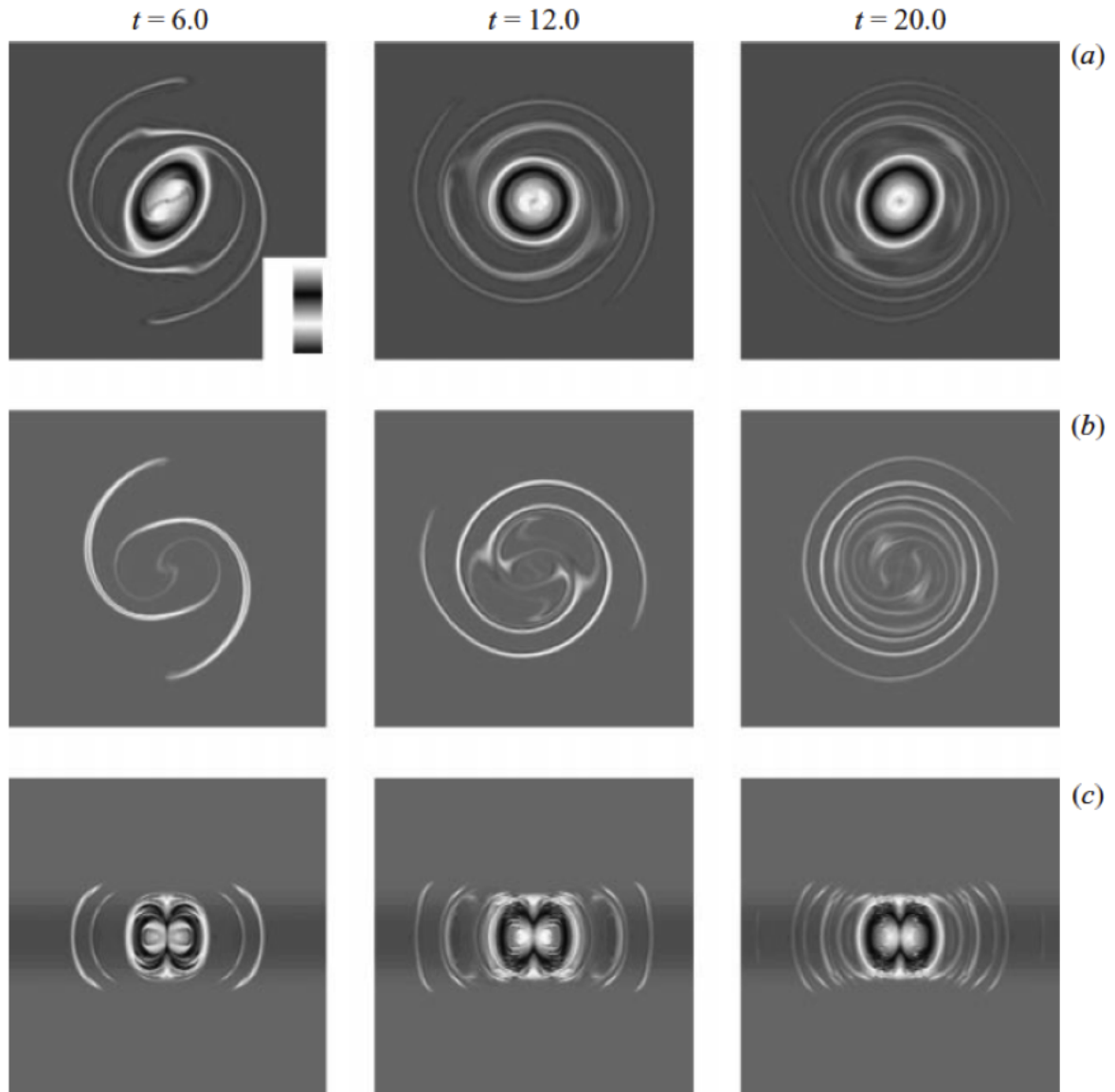


Figure 2: Potential vorticity distribution for baroclinic merging with vertical aspect ratio  $H/R= 1.5$  at times  $t = 6, 12, 20$ . (a) Horizontal sections of potential vorticity on the mid-plane  $z'_c = D/2$  (b) horizontal sections of potential vorticity on the plane  $z'_1 = D/2 + 3H/4$  (c) vertical sections of potential vorticity on the plane  $(x,z)$ .

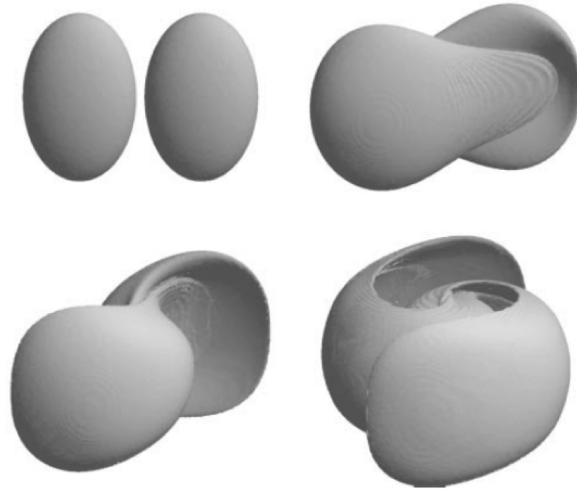


Figure 3: Volume rendering of potential vorticity at time  $t=0, 1, 2, 4$  for baroclinic merging with  $H/R = 1.5$ .

At larger aspect ratio ( $H/R = 2.5$ ), there is not much difference in the structures and the merging dynamics when compared with the case when  $H/R = 1.5$ . However, at low aspect ratios some interesting new features are observed in the outer filaments. Figure 4 shows the (a) horizontal (b) vertical sections of PV field at 3 different time instances. The aspect ratio  $H/R$  is 0.66 in this case. A horizontal section at  $z'_c = D/2$  shows the merging of vortices forming a central core along with the shedding of thin filaments. At a later time, these vortex filaments develop secondary instabilities forming small vortices along the filaments. A vertical section of the PV field shows the curvature similar to the large aspect ratio result. The vortices formed by the secondary instability of the filaments are also visible in the vertical section.

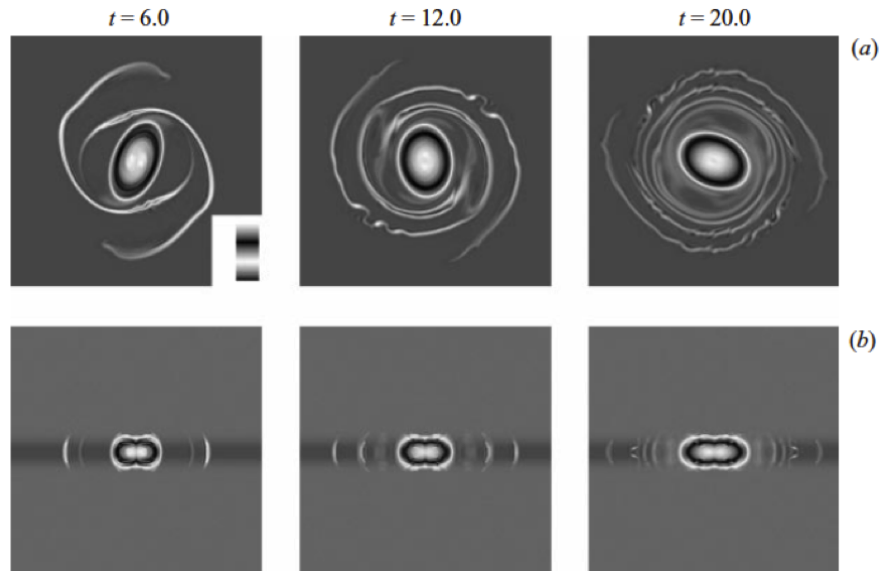


Figure 4: Potential vorticity distribution for baroclinic merging with vertical aspect ratio  $H/R = 0.66$  at times  $t=6, 12, 20$  (a) Horizontal sections of potential vorticity on the mid-plane  $z_c' = D/2$  (b) vertical sections of potential vorticity on the plane  $(x,z)$ .

Next, still lower aspect ratio  $H/R = 0.16$  is considered. The secondary instabilities are very prominent in the outer filaments. Figure 5 shows the horizontal section ( $z_c' = D/2$ ) of PV field at 3 different times. The PV field shows that the filaments are almost destroyed and the newly formed vortices are prominently seen in the outer region.

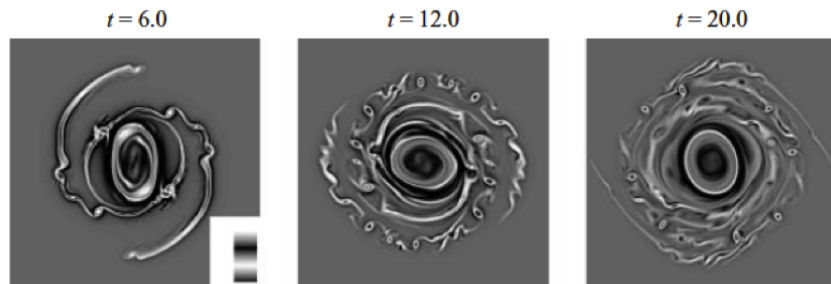


Figure 5: Potential vorticity distribution for baroclinic merging with vertical aspect ratio  $H/R = 0.16$ . The panels show horizontal sections of potential vorticity on the mid-plane  $z_c' = D/2$  at times  $t=6, 12, 20$ .

### 2.3 Lagrangian analysis

Lagrangian analysis provides a good picture of the dynamical evolution of vortex core. The source of fluid particles in the final core (merged) is studied by seeding the tracer particles at two horizontal sections  $z_c' = D/2$  and  $z_1' = z_c' + 3H/4$ . The grey scale in the inset of figures 6(a) and 6(b) indicates the final distance of particles at the end of merging process. At  $z_c' = D/2$ , figure 6 shows that the fluid particles forming the core of the final vortex are originating mainly from the cores of the merging vortices. Outer layers of each vortex move far from the core forming the thin filaments, as discussed before. However at  $z_1'$ , there is no definite core and the particles inside the individual vortices do not play a significant role. Most of the vorticity is distributed in the outer spiral-shaped filaments.

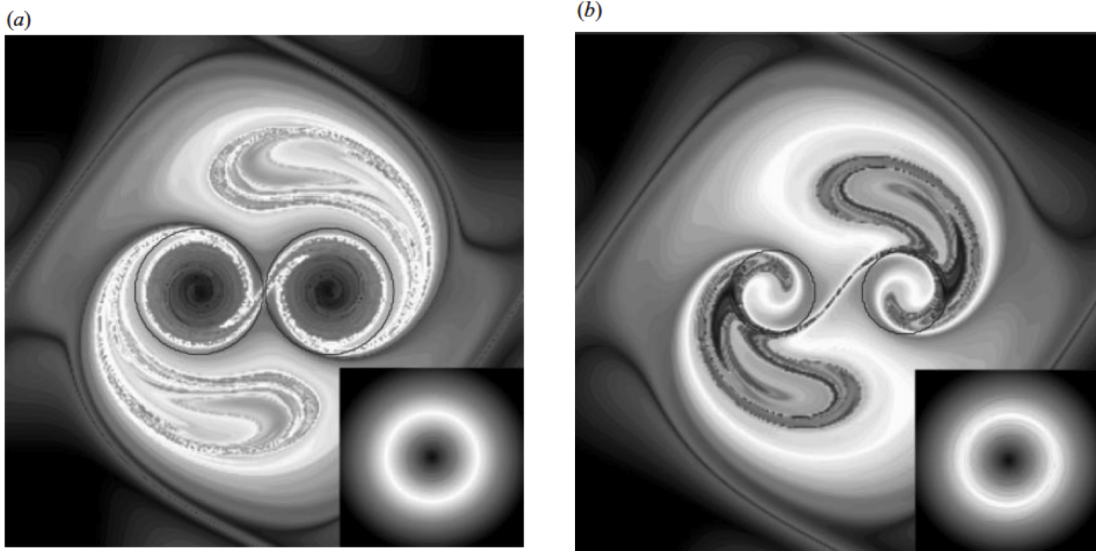


Figure 6: Initial tracer distribution for an aspect ratio  $H/R = 1.5$ . The grey scale indicates the final distance from the center of the domain that the particles will achieve at the end of the merging process, as depicted in the smaller panel inset. (a)  $z'_c = D/2$ , (b)  $z'_1 = z'_c + 3H/4$ .

## 2.4 Critical merging distance

Similar to two-dimensional vortex merging, we expect there to be a critical merging distance between the merging vortices. The dependence of this merging distance on the aspect ratio is presented here. Tracer particles are introduced into the flow with certain number of particles inside each vortex. Merging is considered to be done, when the total number of particles in the suitably defined central region reaches a threshold value which is taken as 99% of the total particles seeded in the flow. Figure 7 shows the graph of critical merging distance as a function of the aspect ratio. Results show that the critical merger distance is influenced strongly by the baroclinicity in the flow. At low vertical aspect ratio, interactions are more local and the critical merging distance is low. For example when  $H/R = 0.66$ , critical merging distance is observed to be  $2.1 R$ . As the aspect ratio ( $H/R$ ) increases the critical merging distance increases rapidly. At very higher values of  $H/R$ , the critical merging distance exceeds that of barotropic vortex merger. Since the vortices here are constrained to have initial conditions which decay in  $z$ , they are never barotropic which could explain this apparent contradiction.

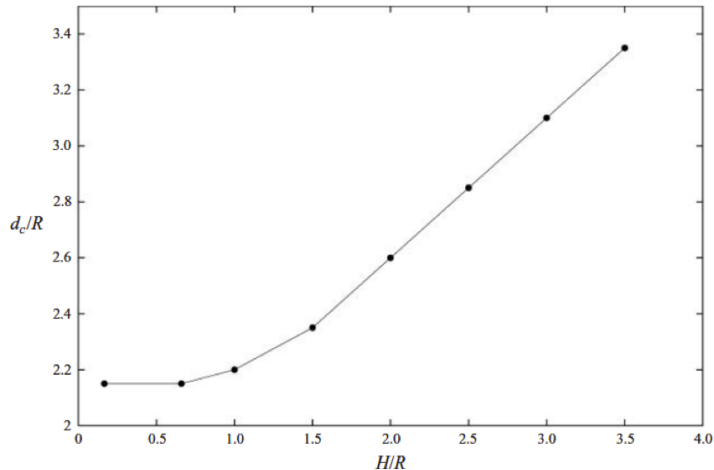


Figure 7: Critical merging distance  $d_c/R$  as a function of the initial vertical aspect ratio  $H/R$ .

### 3 Vortex alignment and merger

Interactions between the ellipsoidal vortices in the three-dimensional quasi-geostrophic turbulence has been studied using the ellipsoidal moment model and the results compared to the numerical simulations [2]. First, we establish the governing equations for the potential vorticity for three-dimensional QG turbulence.

#### 3.1 Ellipsoidal moment model

The equation for the evolution of the potential vorticity  $q$  is

$$\frac{\partial q}{\partial t} + J(\psi, q) = \mathcal{D}, \quad (4)$$

where

$$J(\psi, q) = \frac{\partial \psi}{\partial x} \frac{\partial q}{\partial y} - \frac{\partial \psi}{\partial y} \frac{\partial q}{\partial x}, \quad (5)$$

is the Jacobian operator,  $\psi$  is the stream function and the potential vorticity  $q$  is defined as

$$q = -\nabla^2 \psi = -\left( \frac{\partial^2 \psi}{\partial x^2} + \frac{\partial^2 \psi}{\partial y^2} + \frac{\partial^2 \psi}{\partial z^2} \right), \quad (6)$$

The process of Hamiltonian moment reduction [3] is applied to the three-dimensional QG equations. The equations and the details of this reduction can be found in the appendix section of [2]. The ellipsoid moment model is used to study the interaction of the symmetric vortices. Initial vortex size has been chosen as a spheroid with the aspect ratio of 0.8, which is relevant to the recent QG turbulent simulations [4, 5]. Figure 8 shows the initial positions of the two vortices. The trajectories of the vortices were tracked using an adaptive Runge-Kutta method. Figure 9 shows the trajectories of one of the vortices with two different initial positions.

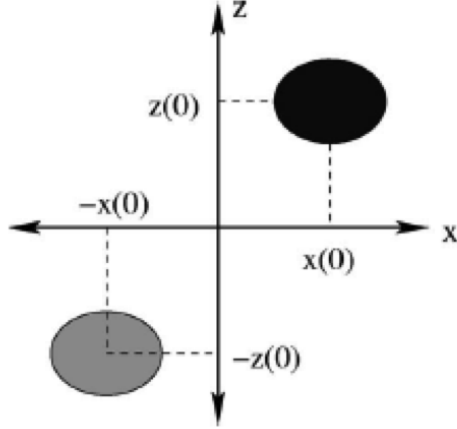


Figure 8: Schematic diagram of the initial positions of the two vortices and the coordinate system used.

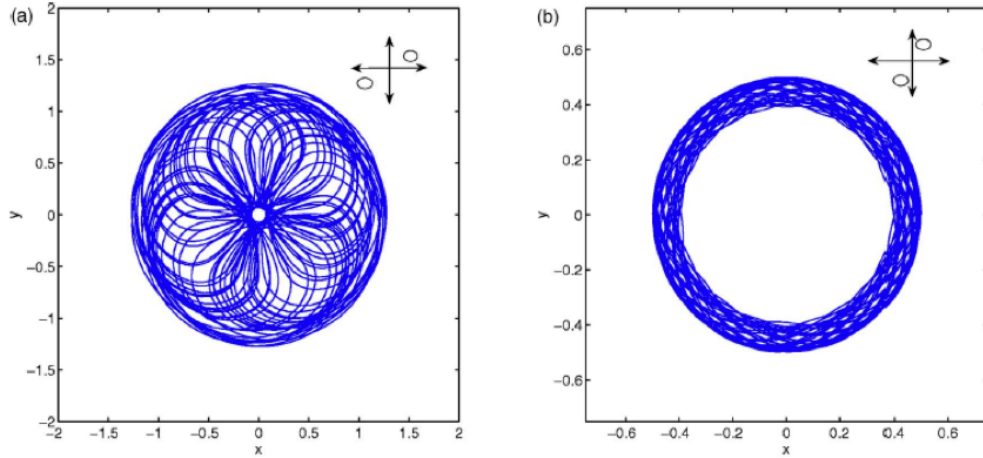


Figure 9: Trajectories projected into the  $x - y$  plane for vortices with initial positions (a)  $x_1(0) = 1.275$ ,  $z_1(0) = 0.175$  and (b)  $x_1(0) = 0.5$ ,  $z_1(0) = 2.0$  as shown schematically in the insets.

### 3.2 Characteristics of merger/alignment

In two dimensions, when the centers of two vortices coincide, the Hamiltonian becomes singular. However, in three-dimensions the centers of vortices never coincide unless they lie on same horizontal plane initially. Based on the trajectories of the ellipsoid moment model, the horizontal separation  $r_h(t) = 2\sqrt{x_1(t)^2 + y_1(t)^2}$ , between the centers of vortices has been considered as the criteria for vortex merging/alignment. The minimum value of horizontal separation  $\mathcal{R} = \min(r_h(t)/r_h(0))$  for different initial positions is shown in figure 10. For larger vertical separations, no sharp transition between merging/non-merging is

observed. In conclusion, there is a sharp transition between merging and non-merging but a smooth transition between alignment and non-alignment.

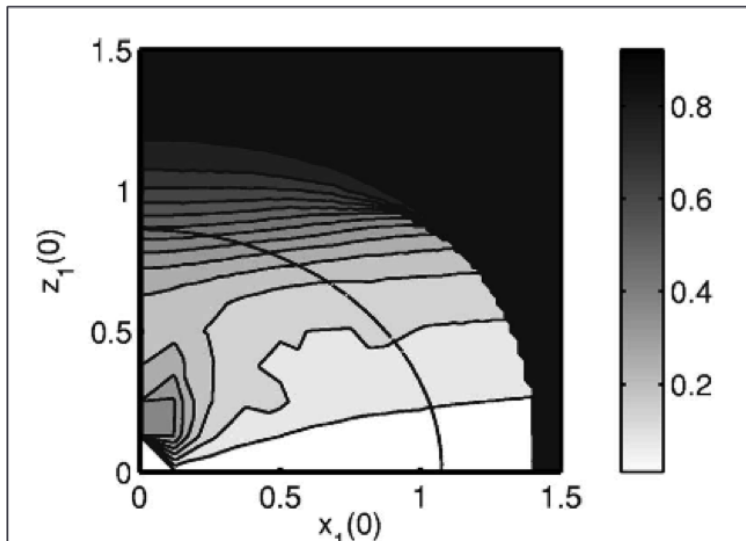


Figure 10: Contours of  $\mathcal{R} = \min_t(r_h(t)/r_h(0))$  for varying initial positions  $[x_1(0), z_1(0)]$ . The solid line is the curve of initial positions that result in two vortices that are initially touching.

### 3.3 Three-dimensional QG simulations

Numerical simulations are performed integrating the three-dimensional QG equations using a fully pseudo-spectral model. Dissipation is included to obtain well behaved numerical solutions. The domain is periodic in all the three directions. Initial conditions for vorticity are chosen such that it matches with the ellipsoidal moment model simulations described above. Vortex merging is observed with small vertical separation and certain critical horizontal separation. Figure 11 shows the evolution of vortex merging in the  $x - y$  plane at different time. Each vortex is seen to have developed a handle which move towards the other vortex along with the formations of filaments. The filaments here dissipate rather quickly because of the non-zero dissipation term. But the total dissipation is not severe, since the the maximum value of the potential vorticity falls to 93% of the initial value at  $t = 500$ . The predictions by the ellipsoidal moment model for the range of initial positions resulting in vortex merging agree well the QG simulation results. The three-dimensional structure of vortices has been investigated in the alignment region to learn about the inviscid behavior of vortices in the alignment region. The evolution of two aligning vortices in a high resolution simulation shows traveling wave-like structures that move up and down the vortex. These waves appear in most of the simulations in the alignment region, which are speculated to be related to the alignment process.

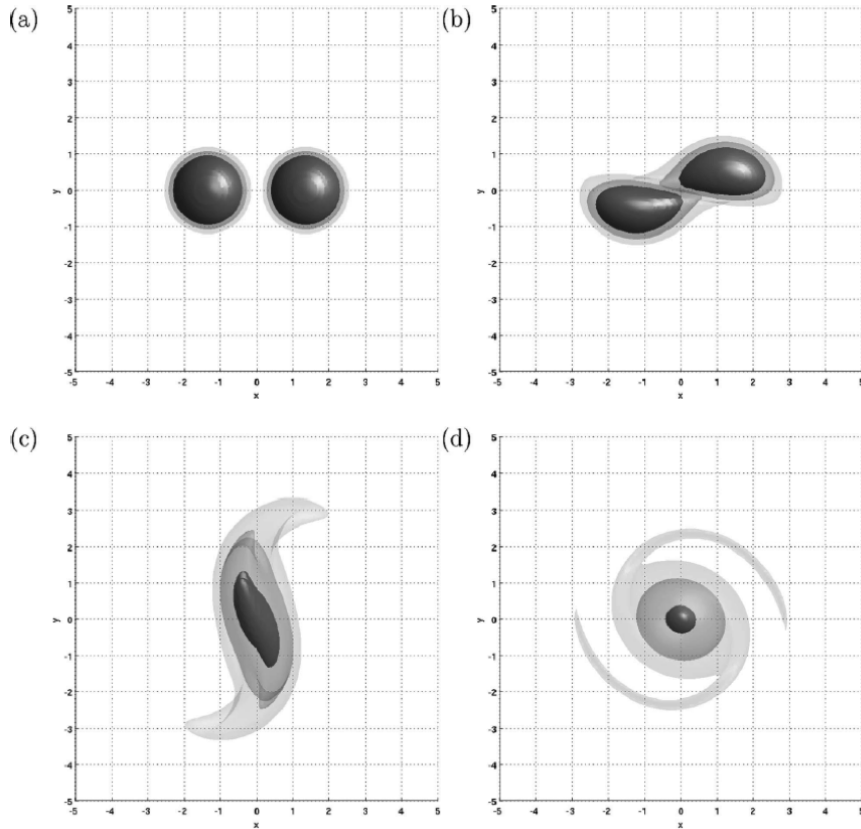


Figure 11: Snapshots of the evolution with  $x_0 = 1.35$  and  $z_0 = 0.3$  at (a)  $t = 0$  (b)  $t = 50$  (c)  $t = 200$ , and (d)  $t = 500$ . The isosurfaces are at 90%, 50%, and 10% of the maximum potential vorticity at that time. The view is looking down the  $z$  axis onto the  $x - y$  plane.

## 4 Conclusion

Numerical studies show that the vortex merging in three-dimensional QG turbulence involves more complex dynamics when compared with the two-dimensional turbulence. The ellipsoid moment model has been used to study the merger and alignment of interacting vortices. Numerical simulations of the QG equations show a good agreement with the ellipsoid moment model regarding the range of initial positions which will result in merging or alignment. Higher resolution simulations and further study of ellipsoid moment model is required to improve the understanding of three-dimensional vortex merging and alignment.

## References

- [1] von Hardenberg, J., McWilliams, J.C., Provenzale, A., Shchepetkin, A. and Weiss, J.B. (1999) Vortex merging in quasigeostrophic flows. *J. Fluid Mech.*, **412**, 331-353.

- [2] Martinsen-Burrell, N., Julien, K. Petersen, M.R. and Weiss, J.B. (2006) Merger and alignment in a reduced model for three dimensional quasigeostrophic ellipsoidal vortices, *Phys. Fluids*, **18**, 057,101114.
- [3] Meacham, S.P., Morrison, P.J. and Flierl, G.R. (1997) Hamiltonian moment reduction for describing vortices in shear, *Phys. Fluids*, **9**, 2310.
- [4] McWilliams, J.C., Weiss, J.B. and Yavneh, I. (1999) The vortices of homogeneous geostrophic turbulence, *J. Fluid Mech*, **401**, 1.
- [5] Reinaud, J.N., Dritschel, D.G. and Koudella, C.R. (2003) The shape of vortices in quasi-geostrophic turbulence, *J. Fluid Mech.*, **474**, 175.